# Influence of Tungsten and Tantalum Content on Evolution of Secondary Phases in 9Cr RAFM Steels: An Experimental and Computational Study

RAVIKIRANA, R. MYTHILI, and S. SAROJA

This paper presents the results of a systematic study on the role of alloying elements W and Ta on the microstructural evolution in 9Cr-W-Ta-V-C Reduced Activation Ferritic/Martensitic steels during long-term thermal exposure in the temperature range of 773 K to 923 K (500 °C to 650 °C). The kinetics of evolution of secondary phases like $M_{23}C_6$, MX, and Laves phase crucially depend upon the W and Ta content of the steel in addition to temperature and time, which has been studied in detail using analytical transmission electron microscopy as well as predictive methods. The steel with 1 wt pct W and 0.06 wt pct Ta showed slow recovery below 873 K (600 °C) and no evidence for Laves phase at any temperature. Significant change in microstructure was observed after 10,000 hours of exposure at 923 K (650 °C), while recovery at short durations was retarded by nucleation of MX precipitates. Increase in both W and Ta content of the steel enhanced the tendency for the formation of Laves phase.

DOI: 10.1007/s11661-017-4136-4
© The Minerals, Metals & Materials Society and ASM International 2017

## I. INTRODUCTION

REDUCED activation ferritic martensitic steels are obtained by the replacement of Mo and Nb by W and Ta, respectively in modified 9Cr-1Mo steel. These steels were developed for nuclear applications in order to reduce the environmental effects during the disposal of irradiated material waste.[1–4] These steels are candidate structural materials for the Test Blanket Module of ITER due to their excellent resistance to radiation-induced swelling, He embrittlement, and improved high temperature mechanical properties[5–9] in the temperature range of 823 K to 873 K (550 °C to 600 °C).[1–9,11]

The physical properties of RAFM steels are similar to that of conventional 9Cr-1Mo ferritic steels. However, due to differences in the chemical composition, the mechanical properties of RAFM steels are superior,[10] which provides an advantage for use at higher operating temperatures. Hence, it is necessary to understand the role of alloying elements, especially W and Ta on microstructural evolution during long-term exposure at temperatures exceeding 873 K (600 °C). The present study aims to understand the phase evolution in steels with different W and Ta contents during thermal exposure using computation methods like JMatPro and is compared with the experimental data. An elaborate study of microstructural and microchemical changes in the steel with 1 wt pct W and 0.06 wt pct Ta with aging in the temperature range of 773 K to 923 K (500 °C to 650 °C) has been made. The influence of varying W and Ta content on the secondary phases like $M_{23}C_6$, MX, and Laves phase has also been studied during accelerated aging at 923 K (650 °C). Correlation of the results obtained from computations as a function of W and Ta content with experimental data showed a reasonable agreement between the estimated phase fraction and composition for different aging conditions.

## II. EXPERIMENTAL PROCEDURE

The steels used in the present study were supplied by M/s MIDHANI Hyderabad, India in the form of 12 mm thick plates. Chemical composition of the steels is listed in Table I. The steels were produced through vacuum induction melting followed by arc refining with a strict control over the purity of raw materials. Specimens of dimensions 10 × 10 × 12 $mm^3$ were normalized at 1253 K (980 °C) for 30 minutes followed by tempering at 1033 K (760 °C) for 1 hour, (N&T) which are used as the starting materials for further experiments. A systematic study on the kinetics of phase evolution as a function of temperature and time was studied in normalized and tempered (N&T) 1W-0.06Ta

RAVIKIRANA is with the Homi Bhabha National Institute, Indira Gandhi Centre for Atomic Research, Kalpakkam 603102, India, and also with the Department of Physics and Nanotechnology, SRM University, Kattankolattur 603203, India. R. MYTHILI and S. SAROJA are with the Metallurgy & Materials Group, Indira Gandhi Centre for Atomic Research, Kalpakkam 603102, India. Contact e-mail: saroja@igcar.gov.in

Manuscript submitted January 16, 2017.
Article published online May 22, 2017

Table I. Chemical Composition of RAFM Steels Studied

| Steel | Element (Weight Percent) | | | | | | | | | | |
|---|---|---|---|---|---|---|---|---|---|---|---|
| | Cr | C | Mn | V | W | Ta | N | O | P | S | Fe |
| 1W-0.06Ta | 9.04 | 0.08 | 0.55 | 0.22 | 1 | 0.06 | 0.0226 | 0.0057 | 0.002 | 0.002 | bal. |
| 1.4W-0.06Ta | 9.03 | 0.126 | 0.56 | 0.24 | 1.38 | 0.06 | 0.03 | 0.002 | <0.002 | <0.001 | bal. |
| 2W-0.06Ta | 8.99 | 0.12 | 0.65 | 0.24 | 2.06 | 0.06 | 0.02 | 0.0024 | 0.002 | 0.0014 | bal. |
| 1W-0.14Ta | 9.13 | 0.12 | 0.57 | 0.22 | 0.94 | 0.135 | 0.033 | 0.0041 | <0.002 | 0.0015 | bal. |

steel, aged in the temperature range of 773 K to 873 K (500 °C to 600 °C) for various durations from 0.5 to 5000 hours. The four (N&T) steels with varying W and Ta content were also subjected to long-term thermal exposure at 923 K (650 °C) for 5000 and 10,000 hours. Hardness measurements were carried out on flat-polished samples using FIE VM-50 PC based Vickers hardness tester at 10 kg load. Transmission Electron Microscopy (TEM) studies were carried out in a Philips CM 200 ATEM (200 kV) fitted with Oxford X-Max SDD detector for Energy Dispersive X-ray (EDX) analysis. Details of sample preparation techniques adopted in this study have been discussed in detail elsewhere.[12]

To understand the precipitation characteristics like volume fraction and microchemistry of secondary phases, simulations were carried out using JMatPro software, which uses CALPHAD-based internal database for the calculation of thermodynamic properties.[13] The input parameters are the chemical composition of the steel, austenitization temperature, and Prior Austenite Grain size. The calculations were performed under the *'General steel'* module in JMatPro® version 7.0.[13] The initial condition for the simulation was assumed to be a single phase martensite structure as in the normalized steel, though 9Cr ferritic–martensitic steels are employed in the N&T condition with a tempered martensite structure. However, the simulation does not take into account this difference in the initial microstructure. Hence, the differences in the results between the simulated and experimental conditions need to be understood in the light of this background. However, the simulation is very useful to obtain valuable details on the sequence of precipitation, for a wide range of compositions and temperature, while experimental data generation over a large matrix is difficult and time consuming. Additionally, simulations can be done for varying time durations, where experiments impose limitations due to kinetic factors. Further, errors associated with experimental data from short exposure times (*e.g.*, <15 minute due to fluctuations in temperature) can be minimized with simulations.

## III. RESULTS

### A. *Characterization of Initial Microstructure*

Thin foil TEM micrograph of normalized and tempered 1W-0.06Ta steel is shown in Figure 1(a). A tempered martensite structure with inter and intralath precipitates is observed. The average lath width was found to be ~370 nm. Based on the detailed analysis of SAED patterns (inset in Figure 1(a)) and EDX spectra (Figure 1(b)), the precipitates have been identified as coarse interlath Cr-rich $M_{23}C_6$ with appreciable solubility for W, Fe, and negligible amount of V; the fine intralath precipitates were either Ta- or V-rich MX with slight solubility of Fe. Composition of $M_{23}C_6$ based on large number of EDX measurements showed average values of 54 wt pct Cr, 18 wt pct W, and 28 wt pct Fe. Average size of $M_{23}C_6$ and MX phases was found to be 120 and 40 nm, respectively.

### B. *Evolution of Secondary Phases: Simulation*

A kinetic simulation of the possible phases during thermal exposure of martensite for 10,000 hours at 923 K (650 °C) in 1W-0.06Ta and 1.4W-0.06Ta steels is presented in Figure 2. In both the steels, metastable phases like $M_3C$, $M_2X$, and $M_7C_3$ are predicted to be stable below 2 hours, while $M_{23}C_6$, MX, and Z-phase are predicted to be stable beyond 10 hours. Laves phase is also predicted in 1.4W-0.06Ta steel, which will be addressed in detail in Section III–B–2. The phase fraction of $M_{23}C_6$ and MX in 1.4W-0.06Ta steel is estimated to be higher than that of 1W-0.06Ta steel, which is understandable owing to its higher W and C content.

The estimated amount of secondary phases in 1W-0.06Ta steel aged for 1000 hours in the temperature of 773 K to 923 K (500 °C to 650 °C) is presented in Figure 3(a). The following inferences are drawn from this figure:

(a) $M_{23}C_6$ is the most dominant precipitate phase followed by MX at any temperature.
(b) Volume fraction of $M_{23}C_6$ and MX increases with temperature up to 850 K (577 °C), beyond which it saturates.
(c) Volume fractions of Laves and Z-phase gradually increase up to 873 K (600 °C), followed by a decreasing trend suggesting their unstable nature at high temperatures. Laves phase is not stable above 923 K (650 °C) in 1W-0.06Ta steel.

Figure 3(b) shows the volume fraction of various secondary phases in the four steels at 823 K and 923 K (550 °C and 650 °C), respectively. It is observed that

(a) Volume fraction of $M_{23}C_6$ is higher in 1.4W steel than in 1W steel at both temperatures, which is mainly attributed to the higher carbon content.

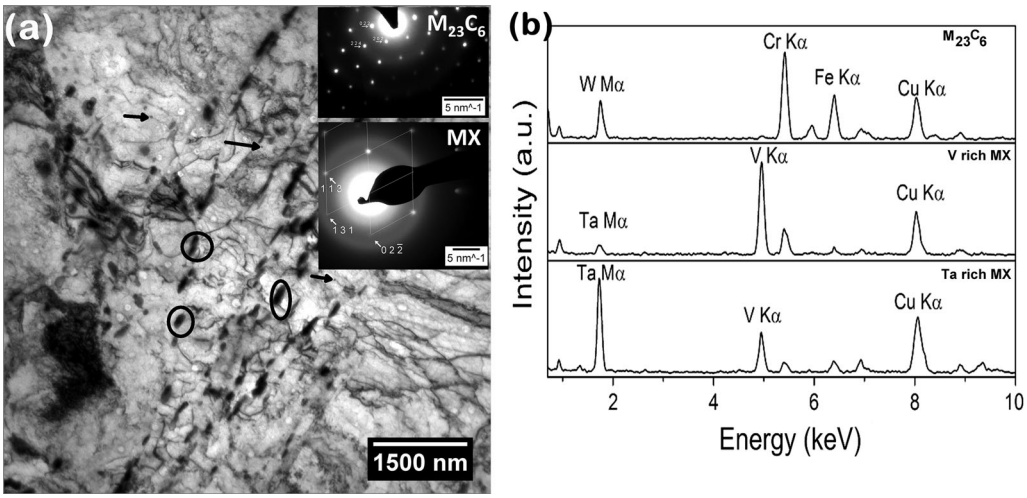


Fig. 1—(*a*) TEM thin foil micrograph of normalized and tempered 1W-0.06Ta steel showing the presence of inter (arrow marked) and intralath (circled) precipitates with insets showing SAED patterns of $M_{23}C_6$ and MX phases along [11-1] and [-411] zone axis, respectively, (*b*) EDX spectra of $M_{23}C_6$ and MX phases.

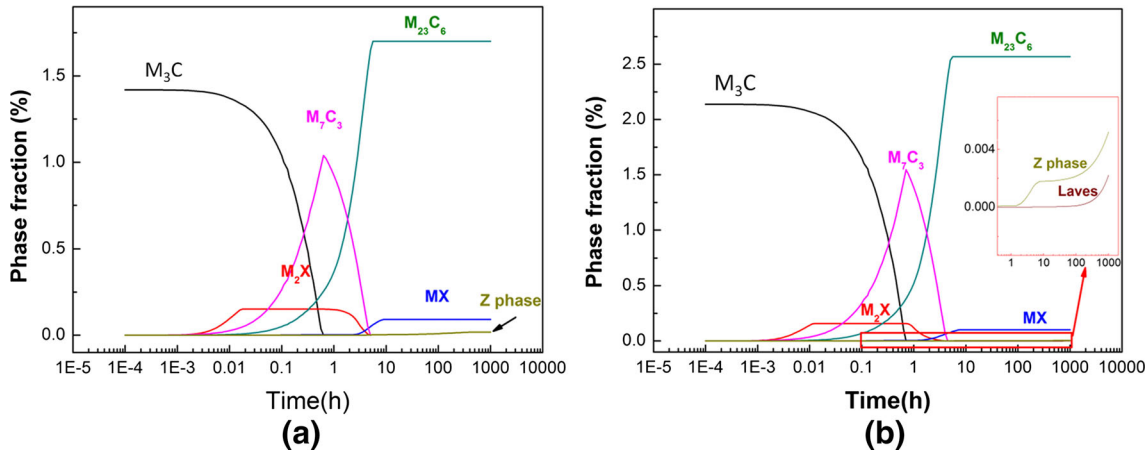


Fig. 2—JMatPro simulation for (*a*) 1W- 0.06Ta and (*b*) 1.4W-0.06Ta steel showing the formation of different secondary phases on aging at 923 K (650 °C).

There is no significant change in the fraction of $M_{23}C_6$ with increasing W concentration beyond 1.4 pct, and also with increase in temperature from 873 K to 923 K (600 °C to 650 °C). Though $M_{23}C_6$ does contain a very small amount of Ta (Figure 4), the increase in phase fraction of $M_{23}C_6$ in the 1W-0.14Ta steel as compared to 1W-0.06Ta steel is mainly attributed to the difference in C content of the steels.

(b) Volume fraction of MX increases as a function of Ta content and does not show a significant change with temperature.

(c) Volume fraction of Z-phase is found to increase with the amount of Ta, but decreases with increase in W content of the steel. However, experimentally Z-phase formation has not been reported in these steels, even under long-term creep conditions, which can be understood in terms of the slow kinetics of Z-phase precipitation that requires dissolution of Ta- and V-rich MX carbonitrides. The absence of Z-phase in Ta-containing reduced activation steels has also been reported by Danon *et al.*[14]

(d) An increase in the volume fraction of Laves phase with increase in W content of the steel is predicted at both 873 K and 923 K (600 °C and 650 °C), with a high concentration at 873 K (600 °C) for 2W steel. The volume fraction of Laves phase predicted after 1000 hours of exposure at 923 K (650 °C) decreases for steels with W ≥ 1 wt pct. Increase in Ta content to 0.14 wt pct is predicted not to favor the formation of Laves phase at these temperatures.

The partitioning of different solutes in $M_{23}C_6$ and MX phases in the temperature range of 700 K to 1000 K (427 °C to 727 °C) is computed by JMatPro for 1W-0.06Ta steel (Figure 4). A high Fe content in $M_{23}C_6$ is seen in this temperature range (Figure 4(a)). The composition of Ta- and V-rich MX carbides could

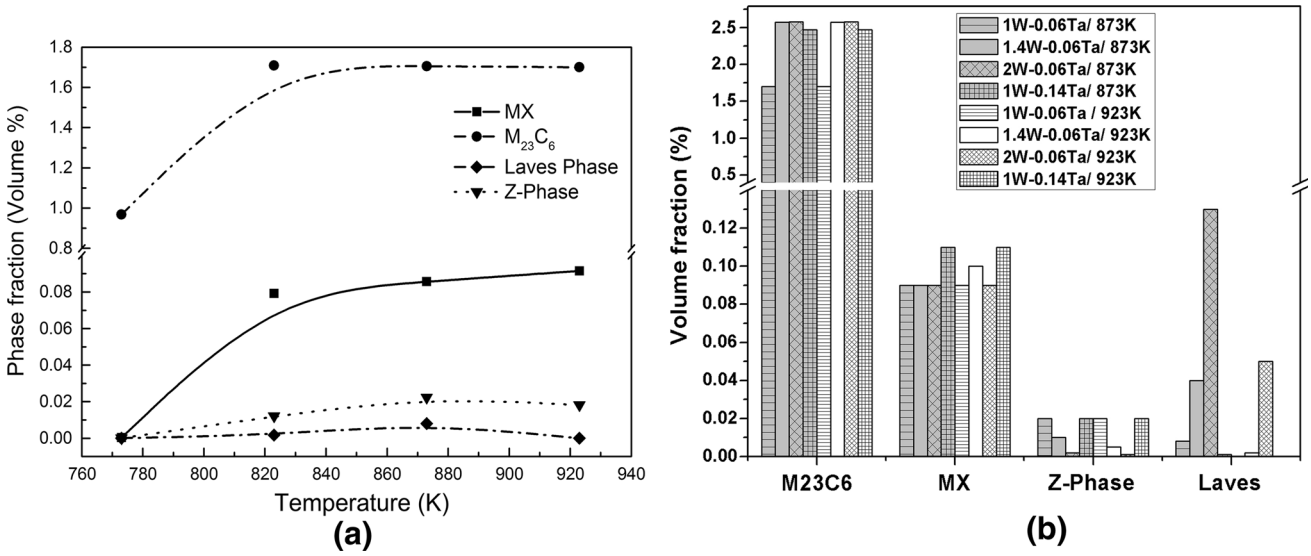


Fig. 3—Volume fraction of secondary phases as a function of (*a*) temperature in 1W-0.06Ta steel and (*b*) steel composition.

**Table II. Chemical Composition (Wt. percent) of Laves Phase in RAFM Steels at 823 K and 923 K (550 °C and 650 °C) Computed by JMatPro**

| | | Steel | |
|---|---|---|---|
| Temperature (K) | Elements | *1W-0.06Ta* | *1.4W-0.06Ta* |
| 923 (650 °C) | Cr | — | 6.4 |
| | Fe | — | 31.1 |
| | W | — | 61.9 |
| | Ta | — | 0.4 |
| | Mn | — | 0.2 |
| 823 (550 °C) | Cr | 7.1 | 6.9 |
| | Fe | 30.3 | 30.6 |
| | W | 61.7 | 61.8 |
| | Ta | 0.6 | 0.5 |
| | Mn | 0.3 | 0.2 |

not be uniquely estimated using JMatPro, although V-rich phase dominates at lower temperature and enrichment of Ta in MX is seen at high temperature (Figure 4(b)). Experimental studies,[12,15–17] have however provided distinct confirmation for the formation of V-rich and Ta-rich MX precipitates, which will be described in the subsequent section.

The composition of Laves phase in 1W-0.06Ta steel in Figure 4(c) shows a constant increase in Fe and W concentrations and a concomitant decrease in Cr and Ta concentrations with increase in temperature in the range of 773 K to 900 K (500 °C to 627 °C). Chemical composition of Laves phase at 873 K and 923 K (600 °C and 650 °C) predicted by JMatPro simulation for the four steels is listed in Table II. The stoichiometry of Laves phase in W- and Ta-containing steels can hence be written as $(Fe, Cr)_2(W, Ta)$, which is in agreement with that reported by Knezevic *et al.*[18]

### C. *Evolution of Microstructure on Long-Term Thermal Exposure*

This section presents the results of the detailed microstructural analysis carried out in the normalized and tempered 1W-0.06Ta steel after aging in the range of 773 K to 923 K (500 °C to 650 °C) for various durations and its correlation to variation in hardness. This section also describes the evolution of secondary phases in other three steels aged at 923 K (650 °C) for long durations of 5000 and 10,000 hours emphasizing the role of W and Ta.

#### 1. *Microstructural evolution and variation of hardness in 1W-0.06Ta steel*

The microstructure of the aged steel did not show significant changes as compared to that of the normalized and tempered steel in the range of 773 K to 923 K (500 °C to 650 °C) on metallographic examination. However, the hardness values showed considerable variation with aging time and temperature, which is described below.

The variation of hardness as a function of time at different temperatures is given in Figure 5. A decrease in hardness with aging time is observed at 773 K and 823 K (500 °C and 550 °C) with a lower hardness at 823 K, understandably due to higher extent of recovery and coarsening of precipitates. On the contrary, there is a peak around 20 hours at 873 K (600 °C), after an initial decrease in hardness up to 5 hours followed by a steady decrease on further aging. Moreover, it is interesting to note that the hardness at 873 K (600 °C) is higher than at 823 K (550 °C). The above results suggest fresh precipitation of secondary phases, which are stable over prolonged durations of thermal exposure. The measured values of hardness at 923 K (650 °C) after 5000 and 10,000 hours of thermal exposure compare with that at 873 K (600 °C). In order to understand the observed trend of hardness especially at 873 K (600 °C), detailed

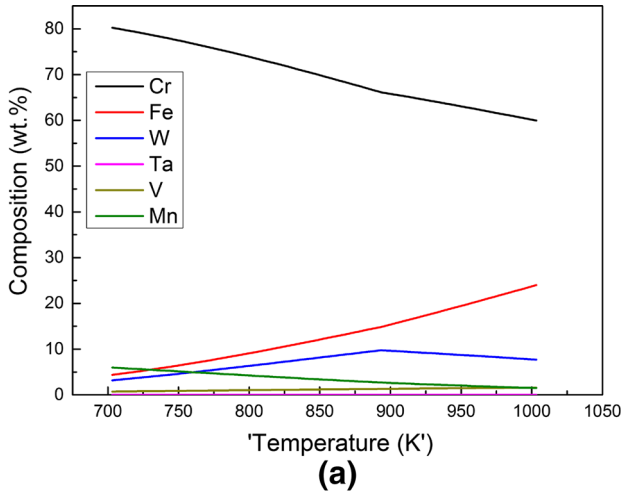


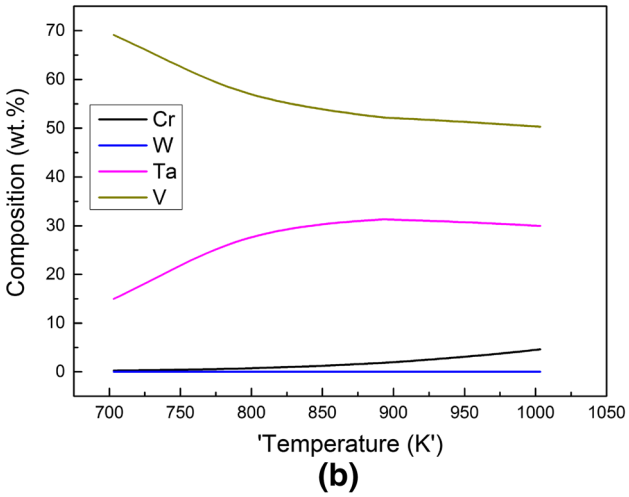


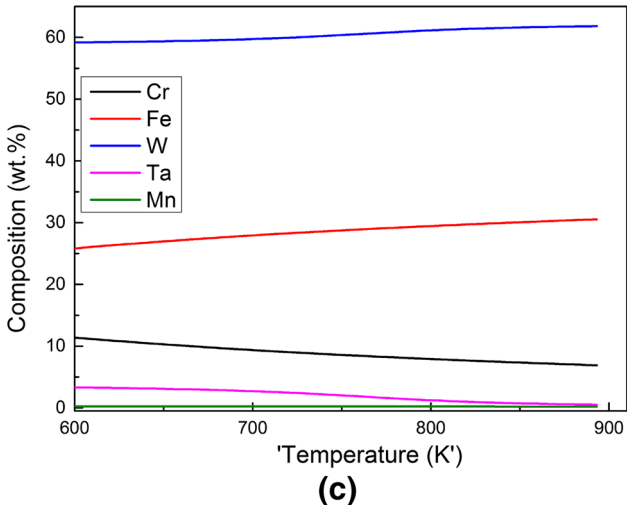


Fig. 4—Composition variation of (*a*) $M_{23}C_6$, (*b*) MX, and (*c*) Laves phase in 1W-0.06Ta steel with temperature calculated using JMatPro.

TEM investigations were carried out, the results of which are described below.

Exposure at 773 K and 823 K (500 °C and 550 °C), as expected did not show significant microstructural changes other than the formation of equiaxed subgrains

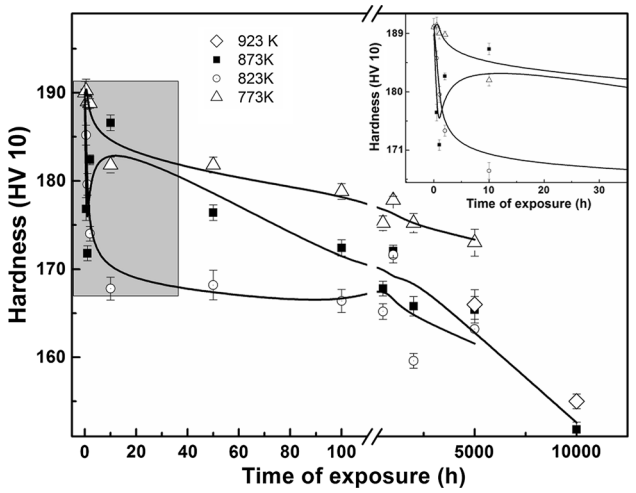


Fig. 5—Variation of hardness of 1W-0.06Ta steel with aging time at different temperatures (inset corresponds to the magnified view of the shaded region).

(size range of 300 to 400 nm) in few regions and retention of lath structure in several regions, typical of partial recovery and recrystallization. The lath width was also comparable to that of N&T steel. The slow recovery of substructure at 773 K and 823 K (500 °C and 550 °C) is only a manifestation of the slow kinetics of diffusion of substitutional elements in α-Fe[19,20] at low temperatures. TEM thin foil and carbon extraction replica micrographs of the 1W-0.06Ta steel aged at 873 K (600 °C) for 10 hours, is shown in Figure 6. It is clearly seen from the micrograph that there is no significant change in the substructure as compared to N&T, while an increase in the number density of precipitates is clearly evident from Figure 6(b).

Thin foil and extraction replica micrographs of 1W-0.06Ta steel aged for 10,000 hour at 873 K and 923 K (600 °C and 650 °C) are presented in Figure 7. An enhanced recovery is observed at 923 K (650 °C) and a decrease in hardness is observed after prolonged exposure up to 10,000 hours. Precipitate size and number density did not change appreciably as function of temperature. However, coarsening of precipitates was observed with prolonged thermal exposure up to 10,000 hours, which is responsible for the decrease in hardness. Formation of Laves phase was not observed in 1W-0.06Ta steel at any temperature, though simulations predicted the formation of Laves phase below 923 K (650 °C).

A comparison of the size distribution of the precipitates as a function of time and temperature is shown in Figures 8(a) through (b), while the variation in the ratio of W/Fe and Cr/Fe in $M_{23}C_6$ is shown in Figure 8(c). An increase in size and decrease in number density of precipitates are observed from Figure 8(a), after 5000 hours of thermal exposure suggesting the coarsening of precipitates. Based on detailed EDX and SAED pattern analyses of large number of particles, it was inferred that the size of Cr-rich $M_{23}C_6$ carbides coarsened up to a size of 200 nm, while that of Ta- or V-rich MX, remained to be in the range of 30 to 50 nm, suggesting its slow

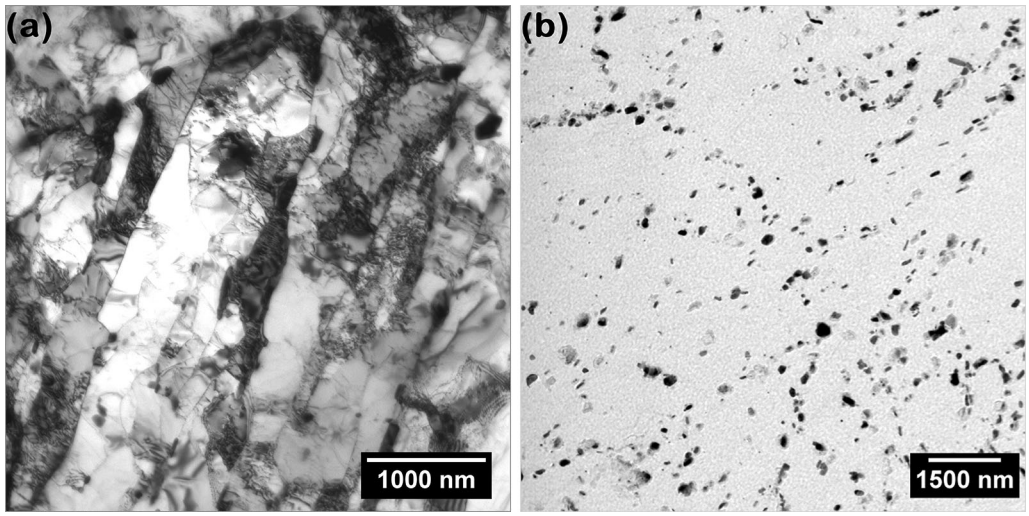


Fig. 6—(*a*) Thin foil and (*b*) carbon extraction replica of 1W-0.06Ta steel exposed at 873 K (600 °C) for 10 h showing insignificant change in substructure and significant increase in precipitate density, respectively.

coarsening as compared to $M_{23}C_6$. Similar observations are also reported in other 9Cr ferritic martensitic steels.[21] Coarsening of precipitates as a consequence of Ostwald ripening[22] was observed with aging time at 773 and 823 K (550 °C), which clearly supports the observed decrease in hardness. Figure 8(b) shows an increase in number density of fine carbides after about 10 hours of thermal exposure at 873 K (600 °C), suggesting the formation of fresh precipitates, which is also supported by a local maximum in the hardness (Figure 5), thus conforming secondary hardening at this temperature. The high hardness observed at 873 K (600 °C) up to 1000 hours suggests that MX type of precipitates nucleated at shorter durations, which are stable and fine over longer aging time and strengthen the matrix unlike $M_{23}C_6$. It is observed that $M_{23}C_6$ although is predominantly Cr rich, it has about 15 to 20 wt pct of W, whose sluggish diffusion being mainly responsible for the fine size and slow rate of coarsening of the carbides.[23] Microchemical analysis of $M_{23}C_6$ did not show appreciable change in the microchemistry at 773 and 823 K (550 °C) (Figure 8(c)), although the Cr concentration is expected to increase[24] with time to achieve equilibrium $Cr_{23}C_6$ composition. With increase in temperature to 873 K (600 °C), an increase in Cr/Fe as well as W/Fe ratio is observed after 1000 hours of aging. Microchemical variation of MX precipitates did not show any particular trend with temperature/time of aging.

2. *Effect of W and Ta on the microstructural changes*

Analysis of thin foil micrographs of 1W-0.06Ta, 1.4W-0.06Ta, 2W-0.06Ta and 1W-0.14Ta steels subjected to thermal exposure for 10,000 hours at 923 K (650 °C) showed the formation of subgrains in the size range of 300 to 400 nm, which did not show appreciable change with W and Ta content.

The carbon extraction replica micrographs of 1.4W-0.06Ta and 2W-0.06Ta steels subjected to thermal exposure at 923 K (650 °C) for 5000 hours are shown in Figures 9(a) and (b). It is observed that there is no change in the average size of MX precipitates with increase in W content (comparison with Figure 7), which is understandable as MX showed no solubility for W. The average particle size of $M_{23}C_6$ decreased from 200 to 170 nm with increase in W content from 1 to 2 pct, confirming that W controls the coarsening of $M_{23}C_6$ precipitates, which is in agreement with the reported results in similar RAFM steels.[4,22] However, quantification of size distribution of the precipitates was difficult in some cases due to agglomeration of precipitates and formation of Laves phase, which is discussed below.

From Figure 9(a), it is observed that in addition to $M_{23}C_6$ and MX, some regions show precipitates with a dark contrast in the close neighborhood of $M_{23}C_6$. EDX analysis in Figure 9(c) of these regions showed enrichment of Fe and W in contrast to Cr enrichment in $M_{23}C_6$. Analysis of the SAED pattern (inset in Figure 9(a)) obtained from such a Fe- and W-rich phase identified it as $Fe_2W$-type Laves phase with HCP structure. The characteristic streaking in the SAED pattern is due to the stacking fault in the Laves phase crystal. The unique microchemistry with enrichment of Fe and W in the Laves phase facilitates its identification, though a low solubility for Ta and Cr was also observed. Figure 9(b) shows the micrograph from the carbon extraction replica of the 2W-0.06Ta steel, aged at 923 K (650 °C) for 5000 hours. With increase in W concentration of the steel to 2 pct, Laves phase formation was found to be more prevalent (Figure 9(b) (arrow marked)), both with respect to size and number density. Further aging up to 10,000 hours showed an accelerated coarsening of Laves phase. Furthermore, Laves phase was found to form like a bridge between $M_{23}C_6$ along the grain boundary, with an average size of the order of 1.5 $\mu$m. As the Ta content was increased to 0.14 pct, the kinetics of Laves phase formation

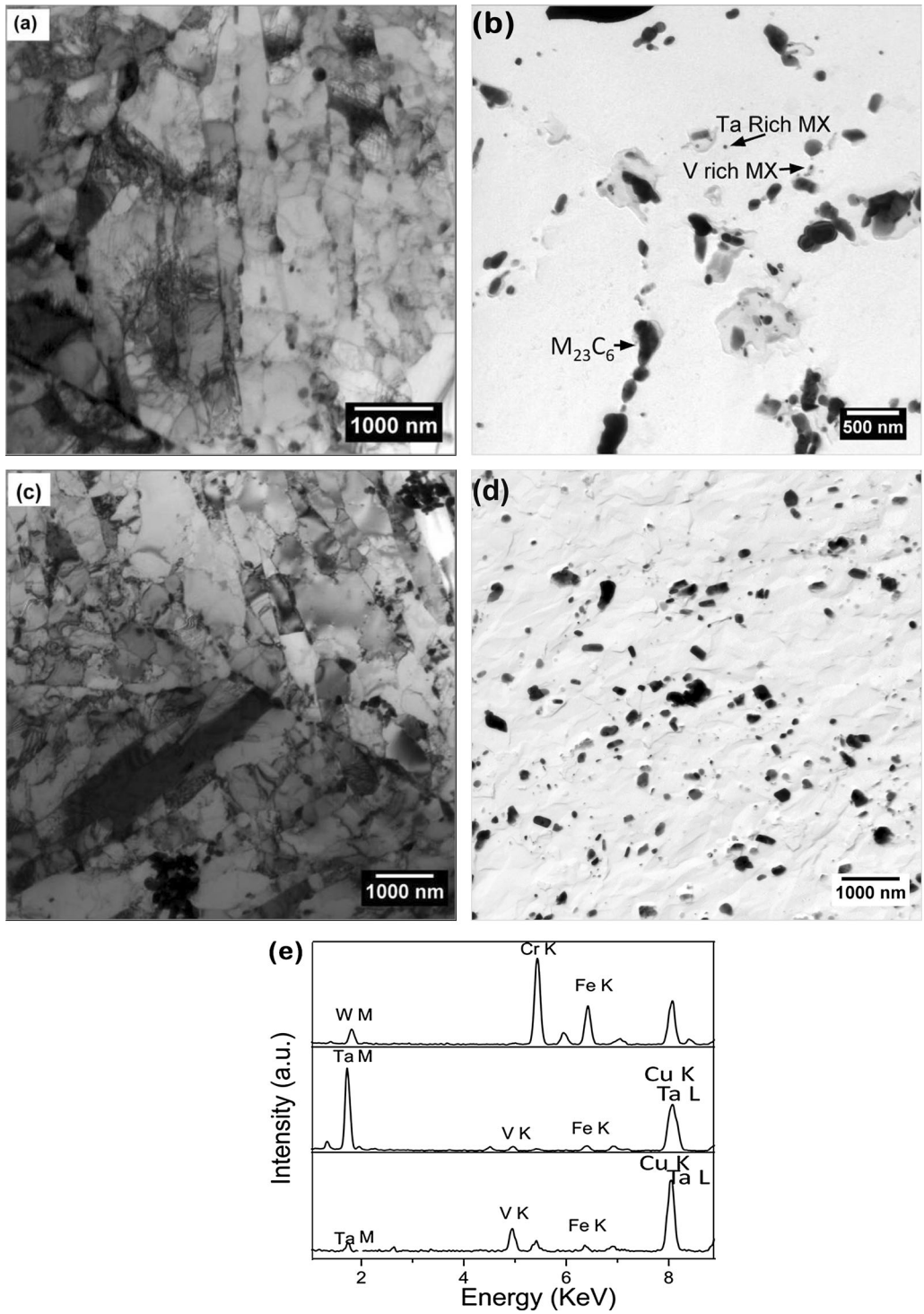


Fig. 7—TEM micrographs of 1W-0.06Ta steel aged for 10,000 h at (*a*, *b*) 873 K (600 °C), (*c*, *d*) at 923 K (650 °C) showing enhanced recovery at high temperature, and (*e*) EDX spectra from the three types of precipitates marked in (b).

showed distinct changes beyond 5000 hours. Typical carbon extraction replica micrograph of 1W-0.14Ta steel exposed to 923 K (650 °C) for 10,000 hours is shown in Figure 10(a). Laves phase was observed after 10,000 hours of thermal exposure at 923 K (650 °C) in this steel in contrast to the 1W-0.06Ta steel. It is interesting to note that the Laves phase in this steel also showed a small amount of Ta in addition to Cr, similar to that observed in 1.4W-0.06Ta and 2W-0.06Ta steels (Figure 10(b)). The mechanism of the formation of Laves phase and the role of Ta are discussed in the next section.

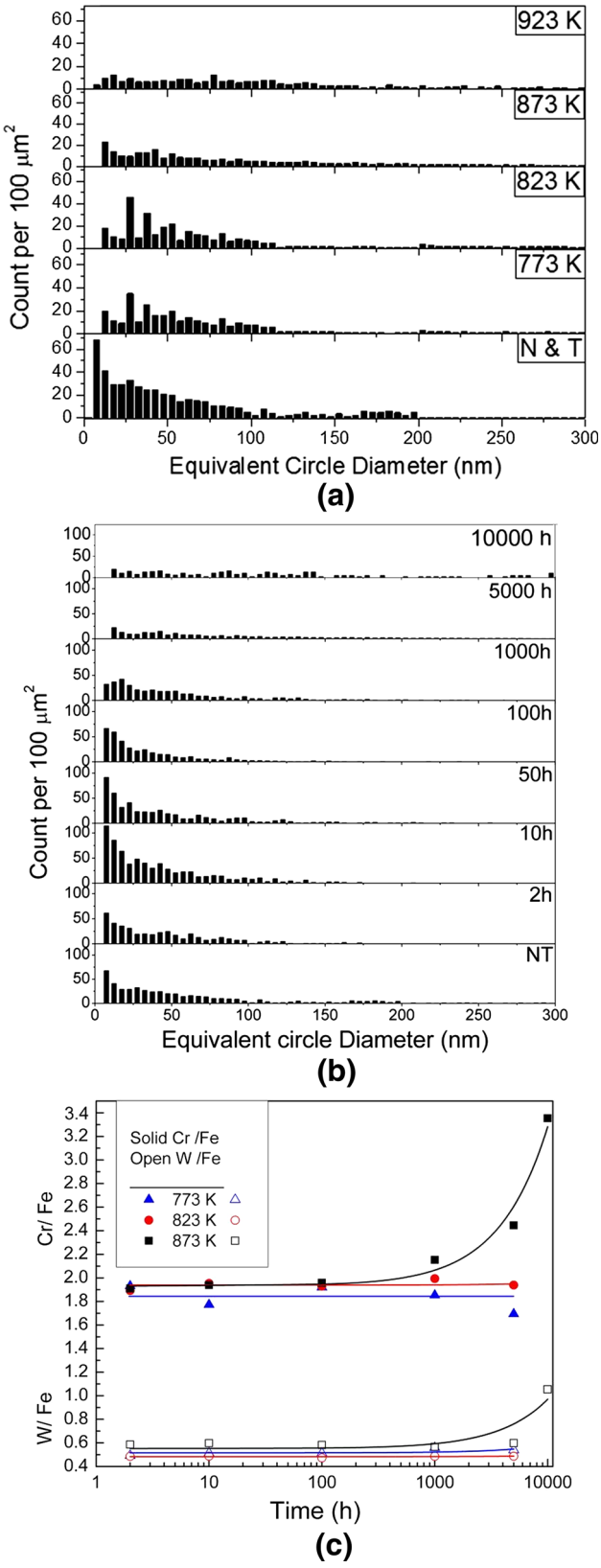


Fig. 8—Frequency distribution of precipitates as a function of size in 1W-0.06Ta steel (*a*) after 5000 h of thermal exposure at different temperatures, (*b*) at 873 K (600 °C) for different durations, and (*c*) variation in microchemistry of $M_{23}C_6$ with time at different temperatures.

## IV. DISCUSSION

### A. *Evolution of Secondary Phases*

The systematic decrease in hardness as a function of time at 773 K and 823 K (500 °C and 550 °C) for the 1W-0.06Ta steel is as expected due to softening of the matrix associated with the recovery of martensite structure and coarsening of precipitates. The secondary hardening observed at 873 K (600 °C) is clearly due to the pinning effect of fine MX precipitates, whose volume fraction increased as seen from the results of simulation and experiments. The near constancy in their size also confirmed their stability against coarsening as compared to $M_{23}C_6$. Formation of equiaxed subgrains at 873 K and 923 K (650 °C) is due to the continuous evolution of microstructure at these elevated temperatures, while the presence of fine subgrains until 5000 hours is attributed to the fine and stable MX, whose number density increased beyond 10 hours of thermal exposure, which also explains the high hardness at these temperatures. The observed reduction in hardness at very long aging times of 10,000 hours is due to the higher extent of recovery and recrystallization at elevated temperatures.

The precipitation of $M_3C$ and $M_2X$ carbides predicted through the computational methods could not be identified in the present experiments. However, the presence of Fe-rich $M_3C$ carbides in normalized steels reported in our earlier study[25] supports the possibility of metastable precipitates in the matrix. Absence of Fe-rich carbides in the normalized and tempered and aged samples indicates that these precipitates are unstable at longer times.

Based on the EDX analysis, chemical composition of $M_{23}C_6$ with temperature showed an increase in Cr and decrease in Fe concentrations and hence the Cr/Fe ratio. However, the microchemical variations in Figure 8(c) show insignificant change in Cr/Fe and W/Fe ratio at 773 K and 823 K (500 °C and 550 °C), which is attributed to the low diffusivity of Cr and W at these temperatures, while at 873K (600 °C) there is an observable increase in the ratios with increasing times. Literature reports for plain and modified 9Cr-1Mo steels[21,26] also showed a progressive increase in Cr/Fe ratio, while Mo/Fe ratio did not show a significant change with time in the temperature range of 773 K to 873 K (500 °C to 600 °C). The increase in Cr/Fe ratio at higher temperature is contradictory to the results from the JMatPro calculations. This discrepancy is due to the way the composition of a phase is calculated in JMatPro. While absolute composition of a phase is determined by EDX analysis, calculations give the distribution of the amount of various elements among the different phases at a temperature for a steel of given composition.

The formation of Laves and Z–phase predicted by JMatPro simulation could not be confirmed by experiments in 1W-0.06Ta steel in the temperature range of 773 K to 923 K (500 °C to 650 °C). This discrepancy between the experimental and simulation results has been reported by Danon *et al.*[14] also in 9Cr-1W-0.18V-0.1Ta-0.125C steel, which is attributed

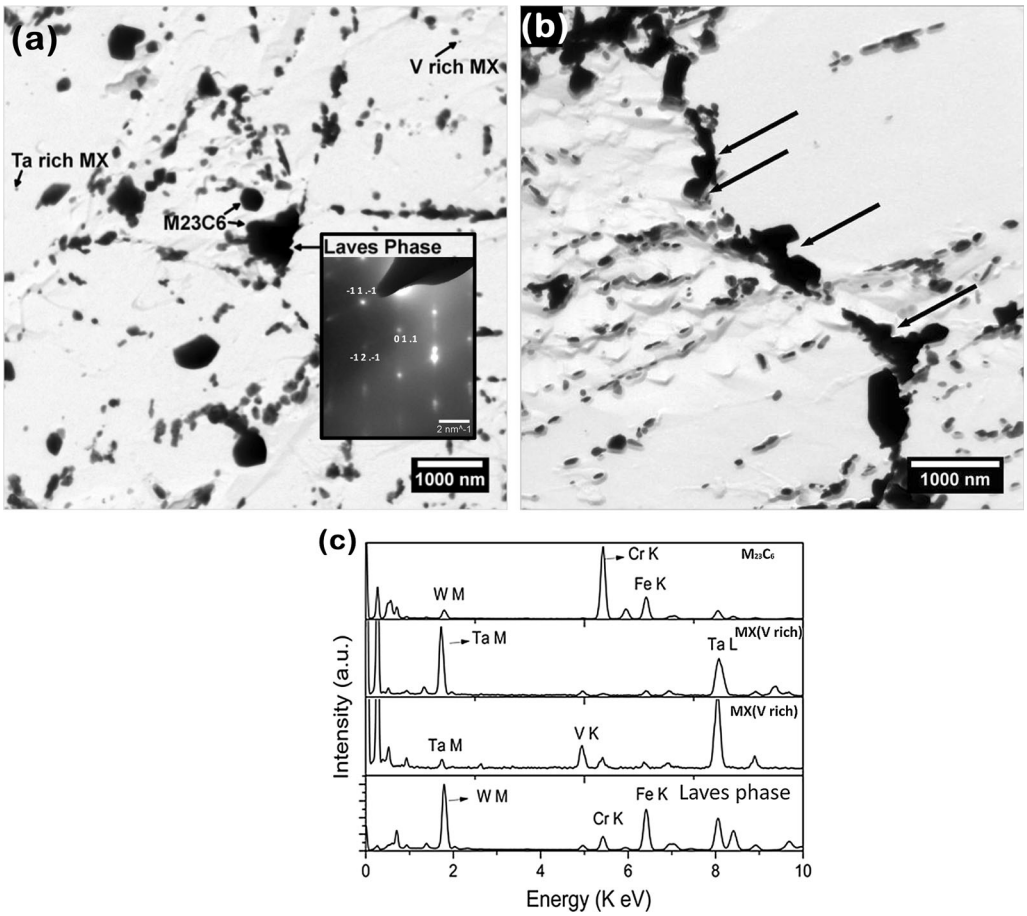


Fig. 9—Extraction replica micrograph of (*a*) 1.4W-0.06Ta with inset showing SAED pattern of Laves phase along [10.−1] zone axis, (*b*) 2W-0.06Ta steel after 5000 h of aging at 923 K (650 °C)- Bridging of Laves phase (arrow marked) is evident in (b); (*c*) EDX spectra of different precipitates marked in (a) showing the enrichment of Fe, and W in Laves phase.

to the enhanced stability of $M_{23}C_6$ due to dissolution of a small amount of Ta, which in turn retards the formation of Laves phase, especially in steels with low W content. The formation of Fe- and Mo-rich Laves phase has been reported by Thomas *et al.*[21] in P91 steel aged for 5000 hours at 823 K (550 °C). Hence, it can be unambiguously concluded that the replacement of Mo by W in RAFM steels delays the formation of Laves phase. Although the formation of Cr- and Nb-rich Z-phase has been reported in Nb-containing steels such as P91, both during thermal and stress exposures, it has not been reported in Ta-bearing steels,[14] which supports the results of the present study.

Based on the results of the present study the following conclusions can be drawn:

- Laves phase formation is delayed by the addition of W as compared to Mo-containing steels.
- Simulations predicted the formation of Laves phase at lower aging temperatures of 773 K and 823 K (550 °C) in 1W-0.06Ta steel, although no evidence was obtained by experiments, which is understood in terms of kinetic factors.
- Volume fraction of Laves phase increased at 923 K (650 °C) with increase in W content above 1 wt pct, which is also supported by literature.[27–31]

Studies on Laves phase formation in W-containing steels have shown that strengthening due to the addition of W is effective only up to an Mo equivalent of 1.5,[32] beyond which ductility of the steel and solid solution strengthening effect of W are drastically reduced, due to accelerated coarsening of the Laves phase. Further, formation of Laves phase in Mo-containing steel is also reported to be dictated by the Mo to C ratio.[33] It is reported that formation of Laves phase is favorable for Mo to C ratio exceeding 5. Along similar lines considering the Mo equivalent expression,[34] this ratio for 1W-0.06Ta and 1W-0.14Ta steels is 6.25 and 7.83, respectively, which should have favored the Laves phase. Hence, the delay can only be attributed to kinetic aspects associated with the lower diffusional mobility of W in ferrite matrix as compared to Mo. However, formation of Laves phase in 1W-0.14Ta steel suggests that the addition of Ta above 0.06 wt pct promotes the formation of Laves phase. It is worthwhile to mention that as per the theoretical calculations of Danon *et al.*,[14] the amount of Laves phase increases linearly up to 1 wt pct Ta more so for Eurofer composition with 9 pct Cr and 1 pct W than for F82H with 8 pct Cr and 2 pct W. It has also been reported[35] that increase in Cr decreases the solubility of Ta in Fe, thereby enhancing

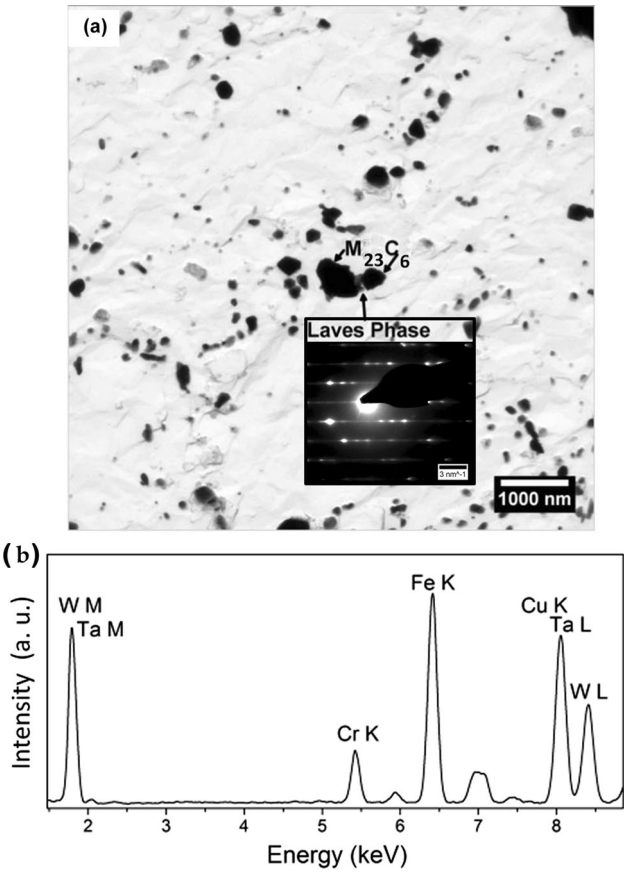


Fig. 10—Extraction replica micrograph of 1W-0.14Ta steel aged at 923 K (650 °C) for (*a*) 5000 h, (*b*) 10,000 h showing Laves phase precipitation with increase in Ta content of the steel after 10,000 h, (*c*) SAED pattern of Laves phase marked in (b) with [10.0] zone axis (*d*) EDX spectra from the Laves phase marked in (b).

the formation of Laves phase. Hence it can be concluded that the possibility of Laves phase formation in 9 pct Cr RAFM steels increases with Ta content.

### B. *Mechanism of Formation of Laves Phase*

The predicted composition of the Laves phases listed in Table II is in agreement with the experimental findings described in Section III–C, which also showed the solubility of small amount of Cr and Ta in addition to the major constituents of Fe and W. However, simulations provided no information on the site of nucleation and the mechanism of formation of Laves phase, which has been attempted through X-ray mapping in an analytical TEM. The carbon extraction replica micrograph of the 2W-0.06Ta steel aged for 5000 hours at 923 K (650 °C) is shown in Figure 11. A chemical mapping (X-ray mapping) on the same region shows the presence of Cr, Fe, W, Ta, and V (Figures 11(b) through (e)). Further image analysis on the X-ray maps revealed the presence of Fe- and W-rich phase surrounding the Cr-rich phase. This suggests that the Laves phase forms around a $M_{23}C_6$ particle. It is clear from the mapped region that $M_{23}C_6$ contains predominantly Cr along with small amounts of Fe, W, and V, while the Laves phase contains large amounts of Fe and W, in addition to small amounts of Cr and Ta.

The above results suggest the heterogeneous nucleation of Laves phase possibly with a chemical interaction with the existing $M_{23}C_6$ during its evolution. Evidence for the existence of isolated particle of Laves phase without the $M_{23}C_6$ phase could not be obtained, which supports the interaction between the two phases.

The effect of higher W was reflected in the increased precipitation of Laves phase in 2W-0.06 Ta steel, while the small amounts of Cr and Ta implies the substitution of Cr in Fe and Ta in W lattices as discussed earlier. This also provides an explanation for the enhanced kinetics of Laves phase formation in the 1W-0.14Ta steel as against its absence in 1W-0.06 Ta steel. The solubility of Cr in Mo-rich Laves phase has been reported in P91 steel by Thomas *et al.*,[21] which supports the present observations. The presence of Laves phase in close association with $M_{23}C_6$ is also supported by Sawada *et al.*,[36] Based on these observations, it can be concluded that

- Laves phase nucleates as (Fe, Cr)$_2$(W, Ta) in the interface of matrix and $M_{23}C_6$.
- Laves phase grows by enrichment of W from $M_{23}C_6$ and Fe from the matrix during thermal aging as the phase evolves.
- Laves phase acts as a bridge for the exchange of Cr between $M_{23}C_6$ and matrix for further enrichment of Cr in $M_{23}C_6$ phase.
- Further growth of $M_{23}C_6$, which is covered with Laves phase is restricted due to non-availability of C; however, significant growth of Laves phase was evident with exposure time.
- Increase in Ta content of the steel promotes formation of Laves phase, in the presence of W.

Formation of Laves phase is reported to strengthen the matrix in the initial stages, which also offsets the coarsening of $M_{23}C_6$.[4] However, the rapid coarsening of Laves phase destabilizes the grain boundary,[37] and also depletes the matrix of the beneficial W, thus degrading the strength.

## V. SUMMARY AND CONCLUSIONS

Systematic studies on the evolution of secondary phases in 9Cr-W-Ta-V-C Ferritic/Martensitic steels during long-term thermal exposure have been carried out and the salient results of the studies show that

- The formation of $M_{23}C_6$, MX, Laves phase, and Z-phase was predicted by computation, while experiments showed the formation of $M_{23}C_6$, MX, and Laves phase. Computed chemical composition of $M_{23}C_6$ and Laves phase was found to be a function of aging temperature, which was also supported by the experimental study.
- 1W-0.06Ta steel showed a slow recovery at temperatures below 823 K (550 °C), which accelerated at 873 K and 923 K (600 °C and 650 °C). However, coarsening of subgrains was sluggish at all temper-

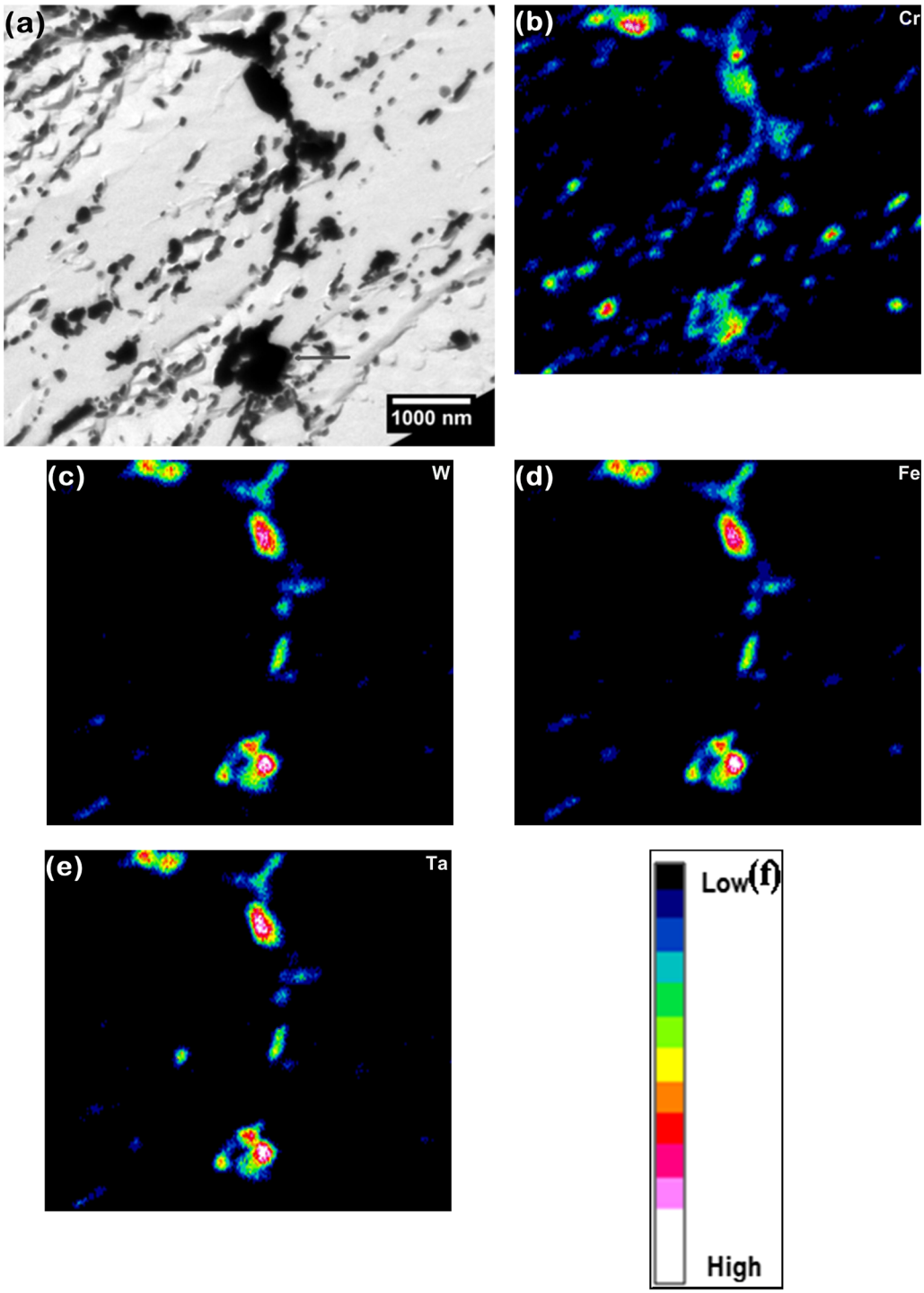


Fig. 11—(*a*) Extraction replica micrograph of 2W-0.06Ta steel aged at 923 K (650 °C) for 5000 h, (*b–e*) elemental maps showing a clear enrichment of W and Fe around the precipitate marked, (*f*) qualitative color code for intensity of different elemental maps shown in (*b–e*).

atures due to the pinning effect of fine precipitates.

- Replacement of Mo by W in RAFM steel retards the coarsening of $M_{23}C_6$ precipitates, which in turn retards the recovery and recrystallization of the fine substructure.
- Presence of fine MX precipitates also helps to retard the substructural recovery.
- Replacement of Mo by W in 1W-0.06Ta steel delays the formation of Laves phase due to the slower diffusion of W in $\alpha$ ferrite as compared to Mo.
- Increase in W content retards the recovery of substructure due to the finer size of $M_{23}C_6$, whereas it enhances the formation of Laves phase.

- Increase in Ta content was not effective in retarding the recovery of substructure as most of the Ta remained in the solid solution, but the formation of Laves phase was enhanced.
- Interaction of Laves phase with $M_{23}C_6$ during thermal exposure has been predicted. Formation of Laves phase around $M_{23}C_6$ restricts the growth of $M_{23}C_6$, whereas the Laves phase coarsens rapidly.
- The computed chemical composition of Fe- and W-rich Laves phase suggested the solubility of small amount of Cr and Ta, which was also evident from the experimental results. Dissolution of Ta in Laves phase was influenced by the W content of the steel.

## ACKNOWLEDGMENTS

The authors sincerely acknowledge Dr. T. Jayakumar, former Director, Metallurgy and Materials Group, IGCAR, Dr. E. Rajendra Kumar, TBM Division, Institute for Plasma Research, Gandhi Nagar, India, and Dr. A.K. Bhaduri, Director, IGCAR, for their sustained encouragement and support. Dr. Ravikirana also acknowledges the Department of Atomic Energy for the award of fellowship, as a part of which this research was carried out.

## REFERENCES

1. R.L. Klueh and D.R. Harries: *High-Chromium Ferritic and Martensitic Steels for Nuclear Applications*, ASTM Monograph, ASTM International, West Conshohocken, 2001, p. 3.
2. F. Abe, T. Noda, H. Araki, and M. Okada: *J. Nucl. Sci. Tech.*, 1994, vol. 1 (4), pp. 279–92.
3. F. Abe: *Sci. Tech. Adv. Mater.*, 2008, vol. 9, pp. 1–15.
4. R.L. Klueh: *Int. Mater. Rev.*, 2005, vol. 50 (5), pp. 287–10.
5. S.N. Rosenwasser, P. Miller, J.A. Dalessandro, J.M. Rawls, W.E. Toffolo, and W. Chen: *J. Nucl. Mater.*, 1979, vols. 85–86, pp. 177–82.
6. D.R. Harries: *Proceedings of Topological Conference on Ferritic Steels for Use in Nuclear Energy Technologies,* Eds. J. W. Davis and D. J. Michel, The Metallurgical Society of AIME, Warrendale, PA, 1984, pp. 141–145.
7. Q. Huang, N. Baluc, Y. Dai, S. Jitsukawa, A. Kimura, J. Konys, R.J. Kurtz, R. Lindau, T. Muroga, G.R. Odette, B. Raj, R.E. Stoller, L. Tan, H. Tanigawa, A.-A.F. Tavassoli, T. Yamamoto, F. Wan, and Y. Wu: *J. Nucl. Mater.*, 2013, vol. 442, pp. S2–S8.
8. K.L. Murty and I. Charit: *J. Nucl. Mater.*, 2008, vol. 383, pp. 189–95.
9. R.L. Klueh and A.T. Nelson: *J. Nucl. Mater.*, 2007, vol. 371, pp. 37–52.
10. A. Alamo, J.L. Bertin, V.K. Shamardin, and P. Wident: *J. Nucl. Mater.*, 2007, vols. 367–70, pp. 54–9.
11. X. Xiao, G. Liu, B. Hu, J. Wang, and A. Ullah: *Mater. Charact.*, 2013, vol. 82, pp. 130–39.
12. R. Ravikirana, S. Mythili, S. Raju, T. Saroja, and E. Jayakumar: Rajendra Kumar*Mater. Charact.*, 2013, vol. 84, pp. 196–204.
13. http://www.sentesoftware.co.uk/jmatpro.aspx.
14. C.A. Danon and C. Servant: *ISIJ Int.*, 2005, vol. 45 (6), pp. 903–12.
15. Ravikirana, S. Raju, R. Mythili, S. Saibaba, T. Jayakumar, and E. Rajendra Kumar: *Steel Res. Int.,* 2015, 86 (7), pp. 825–40.
16. P. Fernandez, A.M. Lancha, and J. Lapena: M, Nernandez-Mayoral: *Fus. Eng. Des.*, 2001, vols. 58–9, pp. 787–92.
17. R. Jarayam and R.L. Klueh: *Metall. Mater. Trans.*, 1998, vol. 29A, pp. 1551–58.
18. V. Knežević, J. Balun, G. Sauthoff, G. Inden, and A. Schneider: *Mater. Sci. Eng.,* 2008, vol. 477A, pp. 334–43.
19. B. Londolt: *Diffusion in Solids, Metals and Alloys*, Springer, Berlin, 1990, p. 372.
20. I. Yoshiaki: *J. Phase Equilib. Diffus.*, 2005, vol. 26 (5), pp. 466–75.
21. V. Thomas Paul, S. Saroja, and M. Vijayalakshmi: *J. Nucl. Mater.*, 2008, vol. 378, pp. 273–81.
22. S. Ghosh: *J. Mater. Sci.*, 2010, vol. 451, pp. 823–1829.
23. Ravikirana, R. Mythili, S. Raju, S. Saibaba, T. Jayakumar, and E. Rajendra Kumar: *Bulll. Mater. Sci.*, 2014, vol. 37 (6), pp. 1453–60.
24. V. Vodarek and A. Strang: *Mater. Chem. Phy.*, 2003, vol. 81, pp. 480–82.
25. R. Ravikirana, S. Mythili, S. Raju, T. Saroja, and E. Jayakumar: Rajendra Kumar: *MaterSci. Tech.*, 2015, vol. 31 (4), pp. 448–59.
26. S. Saroja, M. Vijayalakshmi, and V.S. Raghunathan: *Mater. Trans. JIM*, 1993, vol. 34 (10), pp. 901–06.
27. F. Abe and T. Noda: Okada*J. Nucl. Mater.*, 1992, vol. 195, pp. 51–67.
28. D. Dulieu, K.W. Tupholme, and G.J. Butterworth: *J. Nucl. Mater.*, 1986, vols. 141–143, pp. 1097–1101.
29. Y. De Carlan, A. Alamo, M.H. Mathon, G. Geoffroy, and A. Castailing: *J. Nucl. Mater.*, 2000, vols. 283–287, pp. 672–76.
30. H. Sakasegawa, T. Hirose, A. Kohyama, Y. Katoh, T. Harada, K. Asakura, and T. Kumagai: *J. Nucl. Mater.*, 2002, vol. 490, pp. 307–11.
31. K.W. Tupholme, D. Dulieu, and G.J. Butterworth: *J. Nucl. Mater.*, 1991, vols. 179–181, pp. 684–88.
32. R.L. Klueh: *Elevated-Temperature Ferritic and Martensitic Steels and Their Application to Future Nuclear Reactors,* Oak Ridge National Laboratory, ORNL/TM-2004/176, 2004.
33. O. Prat: *thesis on ''Investigation on Diffusion-Controlled Transformations in Creep Resistant Steels and Grared Cemented Carbides'',* Bochum, 2011.
34. K. Ozaki: *Low Alloy High Steel Tool Having Constant Toughness,* US patent no. US7695576 B2, 13 Apr 2010.
35. K.C. Harikumar and V. Raghavan: *Calphad*, 1991, vol. 15 (3), pp. 307–14.
36. K. Sawada, K. Kubo, and F. Abe: *Mater. Sci. Tech.*, 2003, vol. 19, pp. 732–38.
37. J.S. Lee, H.G. Armaki, K. Maruyamab, T. Muraki, and H. Asahi: *Mater. Sci. Engg.,* 2006, vol. 428A, pp. 270–75.